Published in final edited form as:
Biomaterials. 2015 February ; 41: 166–175. doi:10.1016/j.biomaterials.2014.11.016.

ROS-Responsive Microspheres for On Demand Antioxidant Therapy in a Model of Diabetic Peripheral Arterial Disease

KM Poole[1], **CE Nelson**[1], **RV Joshi**[1], **JR Martin**[1], **MK Gupta**[1], **SC Haws**[1], **TE Kavanaugh**[1], **MC Skala**[1], and **CL Duvall**[1,*]

[1]Biomedical Engineering, Vanderbilt University, 5824 Stevenson Center, PMB 351631, 2301 Vanderbilt Place, Nashville, TN 37235-1631, USA

Abstract

A new microparticle-based delivery system was synthesized from reactive oxygen species (ROS)-responsive poly(propylene sulfide) (PPS) and tested for “on demand” antioxidant therapy. PPS is hydrophobic but undergoes a phase change to become hydrophilic upon oxidation and thus provides a useful platform for ROS-demanded drug release. This platform was tested for delivery of the promising anti-inflammatory and antioxidant therapeutic molecule curcumin, which is currently limited in use in its free form due to poor pharmacokinetic properties. PPS microspheres efficiently encapsulated curcumin through oil-in-water emulsion and provided sustained, on demand release that was modulated *in vitro* by hydrogen peroxide concentration. The cytocompatible, curcumin-loaded microspheres preferentially targeted and scavenged intracellular ROS in activated macrophages, reduced *in vitro* cell death in the presence of cytotoxic levels of ROS, and decreased tissue-level ROS *in vivo* in the diabetic mouse hind limb ischemia model of peripheral arterial disease. Interestingly, due to the ROS scavenging behavior of PPS, the blank microparticles also showed inherent therapeutic properties that were synergistic with the effects of curcumin in these assays. Functionally, local delivery of curcumin-PPS microspheres accelerated recovery from hind limb ischemia in diabetic mice, as demonstrated using non-invasive imaging techniques. This work demonstrates the potential for PPS microspheres as a generalizable vehicle for ROS-demanded drug release and establishes the utility of this platform for improving local curcumin bioavailability for treatment of chronic inflammatory diseases.

1. Introduction

Elevated levels of reactive oxygen species (ROS) cause oxidative stress that contributes to inflammation-related pathologies such as peripheral arterial disease (PAD) [1–3]. Under pathological conditions, leukocytes that are recruited to inflamed sites produce and then release an excess of ROS, causing harm to the surrounding tissues through DNA damage and lipid peroxidation [1, 3, 4]. This process is self-propagating, as the ROS released by inflammatory cells can increase the expression of leukocyte adhesive factors on the

*Tel: (615)322-3598, Fax: (615)343-7919, craig.duvall@vanderbilt.edu.

endothelium, resulting in local extravasation of additional leukocytes that produce additional ROS [5, 6]. Diabetic patients are especially susceptible to oxidative stress and inflammatory diseases, because excessive glucose increases expression of endothelial cell nitric oxide synthase (eNOS) and the production of superoxide, leading to increased generation of hydroxyl radicals, hydrogen peroxide, and peroxynitrite [7–9]. In diabetes, there is a chronic pro-inflammatory environment, where ROS contributes to both endothelial dysfunction and a predisposition to PAD [9, 10]. The strong relationship between hyperglycemia, oxidative stress, and microvascular complications is also supported by observations that compared to the general population, diabetic patients have a four times greater risk of developing PAD [11], worse lower-extremity function [12], and a greater risk of amputation [13, 14]. Furthermore, preclinical studies have shown that animals with type 1 diabetes have an impaired vascular response to ischemia [15–17] and that decreasing oxidative stress improves post-ischemic neovascularization [15, 16]. Therefore, therapeutics that locally reduce oxidative stress have significant potential for treatment of inflammatory diseases like diabetic PAD.

Curcumin, a natural molecule derived from turmeric, is a pleiotropic anti-inflammatory and antioxidant agent that acts through inhibiting the pro-inflammatory transcription factor nuclear factor kappa B (NF-κB) [18, 19] and by scavenging oxidative free radicals through H-atom donation and/or electron transfer [20]. These therapeutic effects would be beneficial for treatment of PAD in the context of chronic, diabetes-induced oxidative stress, and curcumin has shown promise in preclinical ischemia/reperfusion studies [21, 22]. However, therapeutic use of curcumin is limited due to its extreme hydrophobicity which reduces absorption and leads to rapid metabolism and elimination [23]. One approach to overcoming the poor aqueous solubility and stability of curcumin for clinical applications is to deliver it locally from a depot [24]. In order to improve bioavailability of curcumin, sustained/targeted delivery approaches including hydrogels [24], exosomes [25], and stimuli-responsive nanoparticles [4] have been pursued. Microparticles comprising hydrophobic, biodegradable polymers also offer a useful approach for creating an injectable, local depot for controlled drug release [26]. However, conventionally used PLGA-based microparticles are degraded by non-specific hydrolysis and produce acidic degradation products that can exacerbate local inflammation [27] and activate autocatalytic degradation of the particles [28]. This autocatalytic degradation leads to an uncontrolled drug release profile that limits the effectiveness of these particles as vehicles for sustained drug release.

Here, poly(propylene sulfide) (PPS) has, for the first time, been fabricated into microparticles and explored as a candidate for encapsulation and “on demand” delivery of curcumin at sites of oxidative stress. The hydrophobicity of PPS makes it a good candidate for efficient encapsulation of curcumin via oil-in-water (O/W) emulsion methods [26, 29]. Hydrophobic PPS undergoes a morphological transition to more hydrophilic poly(propylene sulfoxide) and poly(propylene sulfone) upon exposure to ROS. Oxidation-responsive polymersomes [30], nanoparticles [31, 32], micelles [33, 34], and hydrogels [35] have been applied; however, there is no example of formulated micron-scale particles that are more effectively retained at the tissue site and generate a stable, local depot for sustained, oxidation-responsive, on demand delivery. This system was designed to leverage the oxidative conversion of PPS to more hydrophilic forms as a trigger for on demand release of

the anti-inflammatory/antioxidant molecule curcumin. The ability to modulate therapeutic release based upon environmental demand [35–38] is anticipated to yield more efficient and sustained local delivery, particularly when applied in the context of diabetic PAD. The studies presented herein include microparticle fabrication and characterization, assessment of on demand release kinetics, and testing for therapeutic effects *in vitro* and *in vivo*. The *in vivo* studies were carried out in the diabetic mouse hind limb ischemia model and showcase new, non-invasive imaging techniques for measuring ischemic limb recovery [39].

2. Materials and Methods

2.1 Materials

All chemicals were purchased from Sigma–Aldrich (St. Louis, MO, USA) and used as received unless otherwise described. Curcumin (368.38g/mol; ≥94% curcuminoid content) was obtained from Sigma. Propylene sulfide was purchased from Acros Organics (NJ, USA) and purified by distillation just before polymerization. 87–90% hydrolyzed poly(vinyl alcohol) (PVA) of average molecular weight 30,000–70,000 was prepared into a 1% w/v solution in deionized water. Transwell inserts with 0.4 μm pore polycarbonate membranes (Corning, Lowell, MA, USA) were used in 24 well plates for curcumin release experiments. SIN-1 was purchased from Invitrogen (San Diego, CA, USA) as a package of 1 mg vials. Cell culture reagents, including fetal bovine serum (FBS), Dulbecco's Modified Eagle Medium (DMEM), and penicillin-streptomycin (p-s) were supplied by Gibco Cell Culture (Carlsbad, CA, USA). 4-Cyano-4-(ethylsulfanyltiocarbonyl) sulfanylpentanoic acid (ECT) was synthesized following the previously reported procedure [40].

2.2 Microsphere Synthesis and Characterization

2.2.1 Synthesis of poly(propylene sulfide) (PPS)—To prepare PPS as previously described [34, 41], propylene sulfide (3.16 mL, 40.4 mmol), ECT (52 mg, 0.20 mmol), TPPCl (tetraphenylphosphonium chloride – $Ph_4P^+Cl^-$) (14.9 mg, 0.040 mmol), and dry NMP (N-methyl pyrolidone) (10 mL) were placed in a dry glass ampoule equipped with a magnetic stirring bar, and the solution was degassed by three freeze-evacuate-thaw cycles. The reaction mixture was stirred at 60°C for 20 hours, and the resulting polymer (Suppl. Fig. 1) was purified by precipitation twice into a large excess of methanol and dried at 60°C under vacuum to yield a red/yellow polymer oil. ^{1}H-NMR ($CDCl_3$, 400 MHz): = 1.25–1.45 (s, C**H$_3$**), 2.5–2.7 (m, C**H**), 2.85–3.0 (m, -C**H$_2$**).

2.2.2 Characterization of PPS—PPS was characterized for molecular weight and polydispersity by gel permeation chromatography (GPC, Agilent Technologies, Santa Clara, CA, USA), and the chemical structure of the polymer was also analyzed by ^{1}H NMR spectra recorded in $CDCl_3$ (Brüker 400 MHz spectrometer). Molecular weight was measured using GPC with DMF + 0.1 M LiBr mobile phase at 60°C through three serial Tosoh Biosciences TSKGel Alpha columns (Tokyo, Japan). An Agilent refractive index (RI) detector and a Wyatt miniDAWN Treos multi-angle light scattering detector (Wyatt Technology Corp., Santa Barbara, CA, USA) were used to calculate absolute molecular weight based on dn/dc values experimentally determined using offline injections into the RI detector.

2.2.3 Microsphere fabrication and drug loading—Curcumin encapsulated PPS microspheres were prepared using a modification of the oil-in-water (O/W) emulsion solvent evaporation method [26, 29]. Briefly, curcumin (20 mg) and PPS (20 mg) were dissolved in a 10:1 mixture of chloroform (1.5 mL) and methanol (0.15 mL) and ultrasonicated (Cole-Parmer, USA) until both polymer and curcumin were completely dissolved to form the oil (O) phase. The 10% methanol was necessary to achieve curcumin solubility. The O phase was then emulsified in 1% (w/v) aqueous PVA solution (6 mL) using an Ultra-Turrax TP 18–10 homogenizer (Janke and Kunkel KG, IKA-WERK) at 20,000 rpm for 1 minute. For solvent removal, the emulsion was then subjected to high vacuum (~635 mm Hg) using a rotary evaporator (Rotavapor RII, BUCHI, Switzerland). Microspheres were then recovered by centrifuging (Allegra X-12 Centrifuge, Beckman Coulter, USA) the remaining aqueous solution at 16,500×g for 5 minutes. The microspheres were then washed once with deionized water and lyophilized (Labconco Freezone 4.5, USA). Unloaded control PPS microspheres were made using the same method described above but without addition of curcumin.

2.2.4 Microsphere characterization—Curcumin encapsulated microspheres were characterized for size and morphology by scanning electron microscopy (SEM, Hitachi S-4200, Hitachi Ltd, Tokyo, Japan). The microspheres were suspended in a water drop and placed on a double sided carbon tape attached to an aluminum stub, air dried, and then sputter coated with gold for 30 seconds. Curcumin encapsulation was confirmed by fluorescent microscopy using a Nikon Eclipse Ti inverted fluorescence microscope (Nikon Instruments Inc., Melville, NY). To do so, microspheres were suspended into a water drop on a glass slide and imaged after covering with a glass cover slip. Drug loading in the microspheres was determined by fully dissolving microspheres in DMSO (1 mg/mL) overnight, centrifuging at 16,500×g for 3 min, and quantifying the curcumin concentration in the supernatant using fluorescence of curcumin (excitation 488 nm, emission 535 nm) in a plate reader (Tecan Group Ltd., Mannedorf, Switzerland). Drug loading and encapsulation efficiency were calculated from the extracted curcumin using established methods [42]. Size of the microspheres was quantified using ImageJ 1.45s software (Freeware, NIH, Bethseda, MD) by measuring SEM diameters of >100 microspheres.

2.3 ROS-Dependent Curcumin Release Kinetics *In Vitro*

In vitro release profiles of curcumin from PPS microspheres were obtained by exposing the PPS microspheres to 0, 0.5, 5, 50, 500, and 882 (3 wt%) mM concentrations of H_2O_2 for 56 days and quantifying the amount of released curcumin by fluorescence (excitation 488 nm, emission 535 nm). PBS (1X, pH 7.4) containing 0.1% w/v N-acetylcysteine (NAC) and 0.01% w/v butylated hydroxytoluene (BHT) was used as the release buffer. Microspheres containing 5 μg curcumin were suspended in 1 mL release buffers with H_2O_2 and placed in the top of transwell inserts (pore size of 400 nm) in 24-well plates. The wells were sealed with parafilm and incubated at 37°C under constant shaking (30 rpm). Releasate was collected from the bottom chamber at regular time intervals and the release buffer was removed and replaced with fresh buffer. Removed release buffer was diluted 2X with 100% ethanol for complete dissolution and evaluated by fluorescence on a plate reader (Tecan Group Ltd., Mannedorf, Switzerland) at excitation 488 nm, emission 535 nm based on a curcumin fluorescence standard curve prepared in the same buffer. Control experiments

were performed after 14 hours of incubation to ensure no effect of H_2O_2 on quantification of free curcumin (data not shown). All release experiments were performed in triplicate. Release experiments were repeated with 3-morpholinosydnonimine (SIN-1) which generates nitric oxide, superoxide, and peroxynitrite [43, 44]. Release buffers containing 0.1 mM, 1 mM, and 2 mM SIN-1 were prepared. In order to measure on demand delivery of encapsulated curcumin, microspheres placed in the top of transwell inserts were subjected to intermittent SIN-1 for 4 day intervals for a maximum of 72 days. Microspheres were subjected to control buffer for 4 days for the “off” phase, and the respective SIN-1 concentration was added at the beginning of each “on” phase of the experiment. Buffer containing SIN-1 was replaced with control buffer at each subsequent “off” interval.

2.4 *In Vitro* Curcumin Delivery

2.4.1 Curcumin-mediated cell survival—NIH-3T3 fibroblasts were transduced with lentivirus to express luciferase (LR-3T3s) as described previously [45]. LR-3T3s were cultured in DMEM supplemented with 10% FBS and 1% p-s, then seeded at 5000 cells/well in a black-walled 96-well plate and incubated at 37°C overnight. The media was replaced with fresh media containing no microspheres, blank PPS microspheres, or PPS microspheres containing curcumin. Varying concentrations of H_2O_2 were added ranging from 0–1 mM. The cells were then incubated at 37°C for 24 hours. Fresh media containing D-luciferin (Biosynth, Itasca, IL) was added to each well at a final concentration of 5 μg/mL, and the luminescence from the viable cells was measured using an IVIS 200 (Xenogen). Luminescence images were analyzed with Living Image® software Version 3.2 (Perkin Elmer).

2.4.2 Cellular internalization of microspheres—3T3 fibroblasts and RAW 264.7 macrophages were seeded in 6-well plates (230,000 cells/well for flow cytometry) or an 8-well chamber cover slip (12,000 cells/well for microscopy) in DMEM supplemented with 10% FBS and 1% p-s and allowed to adhere overnight. Cells were then treated with fresh DMEM with curcumin-loaded PPS microspheres at a curcumin dose of 3.4 μM. One cohort of RAW macrophages were activated to a pro-inflammatory M1 phenotype with 100 ng/mL of LPS and 100 U/mL of interferon-gamma (IFN-γ) [46, 47] to assess the effect of macrophage phenotype on microparticle uptake. All groups were incubated with treatments for 24 hours, then cells were washed 3 times with PBS. For confocal microscopy, cells were imaged in phenol-red free DMEM media with 0.05% trypan blue in order to determine intracellular uptake of microspheres by different cell types. For flow cytometry (FACSCalibur, BD Biosciences), cells were harvested in 0.05% trypan blue in PBS prior to measurement of intracellular curcumin fluorescence.

2.4.3 Macrophage intracellular ROS production in vitro—RAW 264.7 cells were seeded at 230,000 cells/well in 6-well plates in DMEM supplemented with 10% FBS and 1% p-s and were allowed to adhere overnight. Cells were then treated for 1 hour with either blank PPS microspheres or curcumin-loaded PPS microspheres in fresh DMEM medium at a curcumin concentration of 3.4 μM, and then 100 ng/mL of LPS and 100 U/mL of IFN-γ was added to the media prior to an additional 24 hours of incubation to stimulate production of ROS. Control groups consisted of cells without LPS/IFN-γ stimulation and stimulated cells

with no microparticle treatment. After 24 hours of stimulation, cells were washed with PBS and then incubated with 5 μM H2-DCFDA in phenol red-free, serum-free DMEM for 25 minutes. Cells were washed with PBS and harvested in 0.05% trypan blue in PBS. ROS-induced, intracellular fluorescence was measured via flow cytometry (FACSCalibur, BD Biosciences) and analyzed using FlowJo software. Curcumin fluorescence was compensated for using cells receiving the same treatments but without addition of the DCFDA dye.

2.4.4 ELISA to measure effects of curcumin microspheres on MCP-1—RAW 264.7 macrophages were seeded at 20,000 cells/well in a 96-well plate in DMEM supplemented with 10% FBS and 1% p-s and were allowed to adhere overnight. Cells were then treated for 1 hour with either blank PPS microspheres or curcumin-loaded PPS microspheres in fresh DMEM medium (phenol red-free, 1% FBS, 1% p-s) at a curcumin concentration of 3.4 μM, and then the media was supplemented with 100 ng/mL of LPS and 100 U/mL of IFN-γ for an additional 2 hours to stimulate production of ROS. Unstimulated cells were used as a control. After incubation with microspheres and LPS/IFN-γ, the treatments were removed and the cells were given fresh, phenol-red free DMEM (1% FBS, 1% p-s). After 24 hours of incubation, culture media was harvested for measurement of monocyte chemoattractant protein-1 (MCP-1) concentration using an ELISA kit (PeproTech). Protein concentration was normalized to relative cell number using a lactate dehydrogenase (LDH) assay (Promega) performed on lysed cells (KDalert lysis buffer, Life Technologies).

2.5 *In Vivo*

2.5.1 Mouse hind limb ischemia model—Type 1 diabetes was induced in 8-week-old male FVB mice (Jackson Laboratories) with daily intraperitoneal injections of streptozotocin (50 mg/kg) for 5 consecutive days after a 5 hour fast [48]. Glucose levels were measured immediately before induction of hind limb ischemia, and mice with levels above 300 mg/dl were considered diabetic. After 4 weeks of hyperglycemia, hind limb ischemia [49] was surgically induced as described previously [50]. Briefly, the femoral artery and vein of the right hind limb were ligated with 6-0 silk sutures at two locations: immediately proximal to the origins of the superficial epigastric artery and deep branch of the femoral artery, and proximal to the vessels that branch toward the knee. Major side branches were also ligated, and the ligated segment of the femoral artery and vein was excised. The skin incision was closed with interrupted 5-0 nylon sutures. Surgery was performed under isoflurane anesthesia at normal body temperature. Analgesia (10 mg/kg ketoprofen) was administered subcutaneously pre-operatively and every 18–24 hours post-operatively until animals exhibited normal appearance and behavior. At 4 hours post-surgery, the ischemic hind limb was treated with saline, blank PPS microspheres, or curcumin-loaded PPS microspheres at 5 mg/kg curcumin and 10.3 mg/kg PPS via intramuscular injection into the gastrocnemius and adductor muscles (5 × 20 μL injections). Mice were fed a standard chow diet ad libitum and had free access to water. All protocols were approved by the Institutional Animal Care and Use Committee of Vanderbilt University and done in accordance with the National Institutes of Health *Guide for the Care and Use of Laboratory Animals*.

2.5.2 In vivo local retention of curcumin delivered from PPS microspheres—In a separate cohort of mice, hind limb ischemia was induced, and at 4 hours post-surgery, curcumin-loaded microspheres were injected into both the ischemic and control limbs (5 mg/kg curcumin in 10.3 mg/kg PPS) via intramuscular injection. The kinetics of local release of curcumin from PPS microspheres was imaged non-invasively using a Xenogen IVIS 200 to measure curcumin fluorescence (ex: 445–490 nm, em: 515–575 nm).

2.5.3 ROS measurement in extracted gastrocnemius—After 7 days of ischemia, the gastrocnemii of mice from the different treatment groups were extracted immediately postmortem and transferred into PBS in a 24-well plate. A background image of both sides of the gastrocnemius was collected with a Xenogen IVIS 200 (ex: 670 nm, em: 700 nm). The gastrocnemius was then incubated with an ROS-sensitive, fluorescent hydrocyanine dye at a concentration of 100 μM (ROSstar 650, Li-Cor Biosciences, Lincoln, NE) [51] for 45 minutes in the dark then washed with PBS. Both sides of the gastrocnemius were then imaged again with an IVIS 200 (ex: 670 nm, em: 700 nm). ROS was also measured with the hydrocyanine dye method in one untreated animal at day 1 to confirm increased ROS levels in the gastrocnemius at an early time point. The average radiance from the ROS-sensitive fluorescence was quantified for all gastrocnemii images using Living Image® software Version 3.2 (Perkin Elmer).

2.5.4 Intravital hyperspectral imaging of hemoglobin oxygen saturation—Hyperspectral imaging of the footpads was performed at days 0, 2, 4, and 6 post-surgery as described previously [39, 50]. Briefly, a halogen lamp coupled into a liquid light guide provided sample illumination, and the collection arm consisted of a variable focal length camera lens (Navitar, f = 18–108 mm) and liquid crystal tunable filter (CRi, Inc.) mounted on a cooled CCD camera (Andor, 1392 × 1040 pixel). Diffuse reflectance images were collected from 500–620 nm in 8-nm increments and calibrated with measurements of the dark offset and reflectance from a diffuse reflectance standard (Spectralon). Hemoglobin oxygen saturation was then calculated from a modified version of Beer's law that solves for the hemoglobin saturation in each pixel using linear least-squares regression [39, 52–54]. Average hemoglobin saturation values were computed for each footpad by averaging all pixels, and the ischemic footpad measurement was normalized to that of the contralateral footpad.

2.5.5 Perfusion imaging—Perfusion images of the footpads were acquired at days 0, 2, and 7 post-surgery with a commercial laser speckle perfusion imager (Perimed). An average perfusion value was computed for each footpad, and the ischemic footpad perfusion was normalized to that of the contralateral footpad.

2.5.6 Intravital imaging of vascular morphology with optical coherence tomography—At day 7 post-surgery, images of the hind limb vasculature were collected through the skin non-invasively using a swept-source optical coherence tomography (OCT) system with a 1060 nm, 100 kHz source (Axsun Technologies, Inc.) [50, 55]. Speckle variance OCT volumes [56] were collected in a 4 mm × 4 mm area covering the gastrocnemius muscle region to monitor remodeling of vessels in response to hind limb

ischemia [39]. The speckle variance B-scans were processed as described previously [50, 55], and an average intensity projection over ~1.5 mm in depth was computed to visualize all vessels within the volume in a 2D image. The projection images of the vasculature were filtered to enhance contrast and connectivity [50, 55, 57], and the distribution of vessel diameters in each image was quantified.

2.5.7 Histological evaluation of host response to microspheres—At 7 days post-surgery, the mice were sacrificed and the gastrocnemii were removed, fixed with 10% formalin for 24 hours, and embedded in paraffin. Histological sections (4 μm) were cut and stained with hematoxylin and eosin (H&E) in order to assess the host response to the microsphere injections.

2.6 Statistical Analysis

All data are reported as mean ± standard error of the mean (SEM). Analysis of Variance (ANOVA) with a post-hoc Tukey test for multiple comparisons was used to determine treatment effects and $p<0.05$ was considered significant. For *in vivo* hemoglobin oxygen saturation and perfusion endpoints, an ANOVA general linear model analysis with a post-hoc Tukey test for multiple comparisons was performed to determine the treatment effect over the full time course. For comparisons between groups within individual time points, a Wilcoxon Rank Sum test was performed.

3. Results

3.1 Microsphere Synthesis and Characterization

3.1.1 Synthesis and characterization of PPS—PPS was synthesized by ring opening polymerization of propylene sulfide using ECT as initiator and TPPCl as catalyst at 60°C through thioacyl group transfer (TAGT) polymerization. The molecular weight and polydispersity of PPS as determined by GPC were M_n = 17,700 g/mol and PDI = 1.36, respectively. The polymer structure was confirmed by ^{1}H NMR spectra recorded in $CDCl_3$: 1.25–1.45 (s, C**H$_3$**), 2.5–2.7 (m, C**H**), 2.85–3.0 (m, -C**H$_2$**). The polymer synthesis scheme and PPS structure are depicted in Supplemental Fig. 1.

3.1.2 Microsphere characterization—Curcumin-loaded microspheres were characterized for size and morphology by SEM (Fig. 1). Measurements from SEM images indicated that the microspheres had an average diameter of 1.33 ± 0.55 μm (mean ± SD, n > 100). Curcumin encapsulation was qualitatively confirmed by fluorescent microscopy. Drug loading and encapsulation efficiency were 49% w/w curcumin/PPS and 40%, respectively, as determined by extraction of the drug from the microspheres using DMSO.

3.2 Curcumin ROS-Dependent Release Kinetics

For *in vitro* release kinetics experiments (Fig. 2A), the rate of curcumin release was dependent on the concentration of H_2O_2. There was little release in the absence of H_2O_2, and only approximately 20% of the curcumin was released over the entire 56-day period in PBS. For other conditions, the rate of release of curcumin correlated to the dose of H_2O_2.

On demand release of curcumin was exhibited by PPS microspheres intermittently exposed to SIN-1 which rapidly degrades (half-life of 1–2 hours [58]) to simultaneously produce nitric oxide and superoxide. These free radicals combine to form the oxidant peroxynitrite [43]. The samples were exposed to SIN-1 off/on cycles for 4 day intervals for a maximum duration of 72 days to assess whether on demand release could be achieved over an extended timeframe. When microspheres were incubated in a range of SIN-1 concentrations, including 1 mM which has been used to mimic oxidative stress conditions *in vitro* [34, 44, 59], a concentration-dependent and on demand release profile was observed (Fig. 2B, green bars = + SIN-1, white bars = no SIN-1). The slope of the release curve was higher during the SIN-1 "on" phases than the "off" phases for all doses tested. Together, the H_2O_2 and SIN-1 release experiments demonstrate ROS concentration-dependent, on demand release of the antioxidant curcumin from PPS microspheres.

3.3 *In Vitro* Curcumin Delivery

3.3.1 Curcumin-PPS microspheres enhance cell survival in vitro—Next, the ability of curcumin-PPS microspheres to salvage cell viability under cytotoxic levels of ROS was assessed. For a low dose of curcumin-PPS (3.4 μM curcumin, 2.5 μg/mL PPS), it was found that microspheres were cytocompatible and showed a significant therapeutic benefit up to 0.5 mM H_2O_2 ($p<0.05$) (Fig. 3A). At this level of ROS, both blank PPS and curcumin-PPS showed a protective effect since PPS itself scavenges H_2O_2 (Fig. 3A, Suppl. Fig. 2) [32]. A higher dose of curcumin-PPS (27.1 μM curcumin, 20.4 μg/mL PPS) was then tested (Fig. 3B). Although approximately 40% baseline toxicity was seen in the curcumin-PPS treated cells in the absence of H_2O_2, there was a greater therapeutic effect with curcumin-PPS under higher levels of ROS (up to 1 mM H_2O_2). Blank PPS microspheres did not rescue cell viability under these higher H_2O_2 concentrations. Together, these data indicate that both blank PPS and curcumin-PPS microspheres improve cell viability under oxidative stress conditions in a dose-dependent manner. Under greater oxidative stress levels, curcumin-PPS is superior to PPS alone. The lower dose of microspheres was sufficient to improve cell survival in 0.5 mM H_2O_2 conditions without baseline cytotoxic effects, so this microsphere dose was selected for use in further *in vitro* experiments.

3.3.2 Microspheres are preferentially internalized by LPS/IFN-γ-activated macrophages—In order to test whether the microparticles may preferentially target activated, phagocytic cells *in vivo* based on their physical characteristics, *in vitro* cellular internalization of curcumin-loaded PPS microspheres was assessed in 3T3 fibroblasts, RAW cells at baseline, and RAW cells activated to a pro-inflammatory M1 phenotype through a combination of LPS and IFN-γ [46, 47]. After 24 hours of treatment, confocal microscopy and flow cytometry qualitatively and quantitatively indicated that stimulated RAWs internalized the microspheres at a significantly higher rate than control cell types (Fig. 4A–B). Confocal microscopy z-stacks confirmed that microspheres were internalized rather than adsorbed to the outside of the cell membrane (Fig. 4A). Quantification of curcumin-PPS microsphere uptake with flow cytometry confirmed that curcumin-PPS microspheres were preferentially internalized by pro-inflammatory M1 macrophages (Fig. 4B).

3.3.3 Curcumin-PPS reduces intracellular ROS levels in vitro—Curcumin-PPS microspheres exerted a functional effect on intracellular ROS levels in RAW cells activated by LPS and IFN-γ. Flow cytometry quantification of intracellular ROS showed that activated RAWs treated with either blank PPS microspheres or curcumin-loaded PPS microspheres had significantly lower levels of ROS than untreated, activated RAWs ($p<0.05$) (Fig. 4C). Additionally, ROS levels in activated RAWs treated with curcumin-PPS microspheres were approximately 50% lower than in blank PPS-treated cells ($p<0.05$) and statistically equivalent to ROS levels in non-activated RAW cells ($p>0.05$).

3.3.4 Secretion of chemokine MCP-1 is reduced by curcumin-PPS in vitro—After characterizing the antioxidant activity of both unloaded and curcumin-loaded PPS microspheres, we sought to confirm that curcumin loading provides additive anti-inflammatory activity relative to blank PPS microspheres through suppression of the NF-κB pathway [18, 19]. To do so, we compared the effect of curcumin-loaded PPS microspheres to that of blank PPS microspheres on secretion of MCP-1, an inflammatory chemokine whose expression is mediated by NF-κB activity [60, 61], in activated macrophages. Curcumin-loaded microspheres significantly reduced MCP-1 secretion in activated macrophages in comparison to blank PPS-microspheres ($p<0.05$) (Fig. 4D).

3.4 Response to Curcumin-PPS *In Vivo*

3.4.1 Curcumin-PPS microspheres are retained locally and reduce ROS levels in the ischemic hind limb muscle—Local retention of curcumin-PPS microspheres in the hind limb muscle was assessed using an IVIS system to non-invasively image curcumin fluorescence over time after induction of hind limb ischemia (n=5 mice, representative time course in Fig. 5A). In the ischemic limb, curcumin was released more rapidly than in the control limb, presumably due to the increased level of ROS present during ischemia. ROS levels are increased in an untreated ischemic muscle as early as 1 day post-surgery as indicated by a greater than 2-fold increase in fluorescence of the ROS-sensitive hydrocyanine dye relative to the control muscle (Fig. 5B). During the 3 week period following surgery, the average curcumin fluorescence signal in the control limb remained ~4.8x greater than tissue background fluorescence, while the average ischemic limb signal decreased from 6.4x to 3.2x greater than background fluorescence by day 3 post-injection then leveled off to 2.6x from day 3 to day 21 as the limb recovered from hypoxia.

After 7 days of ischemia, the levels of ROS-sensitive fluorescence in the extracted gastrocnemius muscles were significantly lower for mice receiving treatment with either blank or curcumin-loaded PPS microspheres relative to the saline-treated group ($p<0.05$) (Fig. 5C). Additionally, there was a statistically insignificant trend ($p=0.07$) for decreased ROS with curcumin-PPS treatment relative to blank-PPS treatment.

3.4.2 Enhanced recovery of blood oxygenation and perfusion in the ischemic limb—Functional recovery from ischemia was evaluated over a one week period in order to assess the therapeutic effect of curcumin-PPS during a time frame in which ROS overproduction in the ischemic limb is known to occur [15, 62]. Hemoglobin oxygen saturation measured non-invasively with hyperspectral imaging (representative images Fig.

6A) is significantly increased in the curcumin-PPS treated group relative to the blank PPS and saline-treated groups over the time course of ischemic recovery (days 2, 4 and 6 combined, $p<0.05$) (Fig. 6B). At day 2, the curcumin-PPS group has a significantly higher hemoglobin saturation ratio compared to the saline group, while the PPS and saline groups are not significantly different across the time course ($p>0.9$) (Fig. 6B). Similarly, perfusion imaging of the footpads indicated that curcumin-PPS microsphere treatment significantly increases recovery of distal blood flow over the time course of one week relative to blank PPS treatment (days 2 and 7 combined, $p<0.05$). At day 2, the curcumin-PPS group has a significantly greater perfusion ratio than the saline and blank PPS groups (Suppl. Fig. 3).

3.4.3 Intravital imaging of vascular morphology in the ischemic gastrocnemius—The effect of microsphere treatments on vessel remodeling in the ischemic hind limb was imaged non-invasively using speckle variance OCT [39, 50, 56]. Representative images in Fig. 7A provide visualization of vessel morphology in the gastrocnemius muscle at day 7 post-surgery, and the diameter distribution for the curcumin-PPS treated mice showed a significant increase in the length of vasculature with diameters between 25 μm and 125 μm relative to the blank PPS microsphere group ($p<0.05$) (Fig. 7B).

3.4.4 Microspheres are histocompatible in the ischemic limb—H&E staining showed that the muscle status was heterogeneous across cross-sections of the ischemic limb gastrocnemius for all treatment groups at day 7 following induction of ischemia (Suppl. Fig. 4). The majority of the muscle fibers within the gastrocnemius appeared healthy, but there were interspersed regions showing significant mononuclear cell infiltration associated with fibrous tissue and apparent muscle fiber necrosis. These observations suggest that some negative tissue response to ischemia and/or tissue damage due to syringe insertion into the muscle was present for all groups but that there was no apparent, deleterious host response to the microsphere treatments.

4. Discussion

Therapies that target oxidative stress and inflammation in ischemic tissue environments have potential to improve the impaired neovascularization associated with diabetes [15, 16]. Curcumin is a promising candidate due to its demonstrated safety in humans and its combined anti-inflammatory and antioxidant properties; however, curcumin bioavailability is limited by low serum and tissue levels (irrespective of administration route), rapid metabolism, and systemic elimination [18, 20, 23]. For local delivery applications, delivery vehicles are needed that can overcome the limitations of bioavailability due to the extreme hydrophobicity and instability of free curcumin under neutral-basic pH conditions [63, 64]. Previous approaches to improving curcumin bioavailability *in vivo* have included exosomes [25] and liposomes [22] for systemic administration, and stimuli-responsive nanoparticles for local injections at sites of inflammation [4]. However, micron-sized particles may be better suited for forming a stable depot for sustained, localized delivery to an ischemic tissue site. In comparison to nanoparticles, microparticles have reduced systemic absorption and are less apt to diffuse away from the injection site, thus providing sustained, local drug release over a longer time frame [65]. Additionally, particles from 0.5 to 5 μm in diameter could be used to selectively target uptake by phagocytic cell types [66–68], as we have

shown *in vitro* in activated macrophages for our particles with an average diameter of 1.3 μm (Fig. 4A–B). Microparticles composed of PLGA have been used to encapsulate curcumin for sustained release as a cancer therapeutic [26]. However, the release kinetics can be affected by PLGA autocatalytic degradation, and the degradation products of PLGA cause a local acidification and inflammatory response [27, 28]. To accomplish the goals of providing sustained, local, on demand antioxidant and anti-inflammatory therapy to ischemic tissues under oxidative stress, we have pursued ROS-sensitive PPS microspheres as a delivery vehicle.

PPS was selected as the vehicle for curcumin in this application because its hydrophobicity allows for efficient encapsulation of hydrophobic curcumin via O/W emulsion, and the cargo is released in a bioresponsive, ROS-dependent manner as shown by exposure of the curcumin-loaded microspheres to H_2O_2 and SIN-1 *in vitro* (Fig. 2). While a bolus delivery of ROS was used for these cell free experiments in contrast to the continuous ROS generation that occurs in inflamed tissues *in vivo*, the ranges of H_2O_2 and SIN-1 doses were selected to include physiologically-relevant ROS concentrations [34] as well as higher doses that demonstrate the ROS concentration-dependency of curcumin release. Though it is difficult to precisely mimic the complex milieu of ROS present *in vivo*, the dose range of peroxynitrite-generating SIN-1 tested in this work corresponds with doses of up to 1 mM SIN-1 that have been used to mimic pathological conditions on cells [44, 59]. While some of the doses of H_2O_2 and SIN-1 used in these drug release studies may be superphysiologic, these results demonstrate that the microspheres respond to multiple sources of ROS which contribute to oxidative stress in inflamed tissues. With regards to the PPS microsphere drug-release mechanism, the hydrophobic sulfide is converted to more hydrophilic sulfoxide/sulfone by ROS-mediated oxidation [30]. We expect that this phase change causes swelling and then gradual disassembly of the PPS microparticle matrix into water soluble, unimeric polymers and that progression of this process triggers release of the microsphere cargo. Unlike PLGA, the byproducts of PPS microsphere degradation do not acidify the local environment [27], and PPS has been safely used as a component in nanoparticle and polymersome drug carriers *in vitro* and *in vivo* [31, 34, 69].

In addition to its cytocompatibility and utility for drug loading, PPS has inherent therapeutic properties as a H_2O_2 scavenger [32]. To our knowledge, our group was the first to demonstrate the cell-protective effects of PPS in the presence of cytotoxic levels of ROS in recent work with PPS-containing hydrogels [35]. We have also observed this benefit here with our PPS microparticle-based injectable drug depot as shown in experiments with 3T3 fibroblasts (Fig. 3 and Suppl. Fig. 2). Importantly, curcumin was synergistic with PPS, and the curcumin-loaded microparticles showed superior therapeutic benefit compared to blank particles under higher H_2O_2 concentrations. In this context, it is presumed that curcumin microparticles injected into tissue would remain within the tissue stroma and release therapeutic curcumin and/or scavenge extracellular ROS to reduce oxidative stress on surrounding skeletal muscle and other resident cells. However, it was also found that fabrication into micron-sized particles enabled preferential curcumin-PPS microsphere uptake by more phagocytic, activated macrophages (Fig. 4A–B), as these particles fall within the size range that is not efficiently internalized by non-phagocytic cell types [66–

68]. This preferential targeting to inflammatory cells is desirable since these cells are the primary producers of damaging ROS and pro-inflammatory signals [1, 3, 5]. Furthermore, ROS may also be produced and accumulate in intracellular compartments such as phagosomes and endosomes/lysosomes [70], and targeting antioxidant enzymes to endocytic vesicles may be an effective approach for quenching endosomal superoxide [71]. Thus, tuning of PPS microparticle size to be optimized for phagocyte internalization may enable direct targeting to ROS at their subcellular source. In the current study, blank and curcumin-loaded PPS microspheres significantly reduced intracellular ROS levels in activated macrophages (Fig. 4C). PPS microsphere-mediated ROS scavenging in living cells is a novel finding for PPS, to our knowledge, and the synergy with curcumin is in agreement with previous studies demonstrating the antioxidant effects of curcumin *in vitro* [4, 72]. Thus, these data suggest that curcumin-loaded PPS microparticles would potentially have a combined mechanism *in vivo* where curcumin would be released extracellularly and also intracellularly primarily within activated, phagocytic macrophages. Curcumin-PPS microspheres also reduced secretion of chemokine MCP-1 in activated macrophages (Fig. 4D), confirming anti-inflammatory activity through inhibition of the NF-κB pathway [60].

Diabetes-induced oxidative stress impairs post-ischemic neovascularization, and reduction of ROS represents a promising approach to remedy PAD [15, 16]. Curcumin is a promising candidate in this context, and it has been shown to have therapeutic benefit in preclinical models of inflammation and ischemia/reperfusion injury using delivery approaches such as systemic injection of free curcumin [21], systemic injection of exosomes [25] and liposomes [22], and local injection of stimuli-responsive nanoparticles [4]. However, sustained, ROS-demanded delivery of curcumin from a local depot has yet to be investigated in a model in which ischemia and ROS production are exacerbated by diabetes. In the current work, we have shown that *in vitro* rate of release of curcumin from PPS microparticles is modulated by environmental levels of ROS such as H_2O_2 and peroxynitrite over a sustained time frame (Fig. 2). This on demand delivery mechanism was also demonstrated *in vivo*. Increased ROS in the ischemic hind limb mediated rapid release of curcumin from PPS microspheres (Fig. 5A–B), while in the normoxic control limb, microspheres were retained at the site of injection without significant drug release over the 21-day time frame tested. The stable curcumin fluorescence signal observed in the control limb over time suggests that the microsphere depot remained intact in the absence of pathological levels of ROS. This on demand release mechanism was also found to have significant ROS scavenging effects *in vivo*, and the curcumin-PPS microspheres significantly reduced ROS in the ischemic muscle 7 days following delivery. In this study, the blank PPS microspheres again showed an intermediate reduction of local ROS (Fig. 5C). These *in vivo* therapeutic studies focused on the acute phase of recovery since the control animals in this model also showed functional improvements at later time points (Fig. 6B and Suppl. Fig. 3). Based on pilot studies in which free curcumin formed crystals *in vitro* (Suppl. Fig. 5A) and exacerbated ROS levels in ischemic tissue (Suppl. Fig. 5B), we did not pursue free curcumin treatments in this work.

The functional effects on vascular recovery in the diabetic mouse hind limb ischemia model were investigated with non-invasive optical imaging techniques [39, 50]. Hyperspectral imaging of hemoglobin oxygen saturation (Fig. 6), perfusion imaging of the footpads

(Suppl. Fig. 3), and OCT of vessel morphology in the gastrocnemius (Fig. 7) revealed that the curcumin-PPS microspheres significantly improved recovery in this model of diabetic PAD. Controlled, on demand release of PPS and curcumin may help keep local levels of ROS within an optimal range, since both too much [15, 16, 73] and too little ROS [62, 74] are detrimental to angiogenesis and ischemic recovery. The greater functional benefit observed from curcumin-PPS microspheres relative to blank PPS particles in this study may be due to the more pleiotropic effects of curcumin in addition to scavenging ROS, including inhibition of NF-κB activity, reduction of proteolytic enzyme levels, inhibition of platelet aggregation, and other anti-inflammatory, antioxidant, and antidiabetogenic effects [18]. Overall, these results are promising for the context of excessive ROS and inflammation in diabetes, and there is an opportunity to optimize dosing and pharmacokinetics *in vivo* to achieve maximal therapeutic benefit.

5. Conclusions

ROS-responsive PPS microspheres were successfully utilized for encapsulation and sustained, on demand delivery of curcumin in the diabetic mouse hind limb ischemia model of peripheral arterial disease. The PPS microspheres were found to be cytocompatible, improved cell survival under exogenous oxidative stress, and reduced ROS levels *in vitro* and *in vivo*. Interestingly, blank PPS microspheres also showed some therapeutic function *in vitro*, although curcumin-loaded PPS microspheres were significantly more effective overall, especially in functional measures of recovery in the ischemic hind limb. The use of PPS microsphere-based environmentally-sensitive depots represents a compelling approach to provide on demand bioavailability of curcumin or other antioxidants for treatment of diabetic PAD or other localized tissue sites affected by chronic inflammatory diseases.

Supplementary Material

Refer to Web version on PubMed Central for supplementary material.

Acknowledgments

The authors thank Constance Lents, Kameron Kilchrist, Jinjoo Lee, Devin McCormack, Megan Madonna, and Chetan Patil for assistance with experiments and image processing, and Lillian B. Nanney for use of the perfusion imager. SEM was conducted through the use of the core facilities of the Vanderbilt Institute of Nanoscale Sciences and Engineering (VINSE). IVIS imaging was performed in the Vanderbilt University Institute of Imaging Science (VUIIS, supported by NCI P30 CA068485). Confocal Imaging was performed using a Zeiss LSM 510 Inverted Confocal Microscope through the use of the VUMC Cell Imaging Shared Resources, (supported by NIH Grants CA68485, DK20593, DK58404, DK59637, and EY08126). This work was supported by a Vanderbilt Discovery Grant, NIH R21 HL109748, and American Heart Association Grant-in-Aid 12GRNT 12060235. K.M.P. was supported by a P.E.O. Scholar Award and an NSF Graduate Research Fellowship DGE-0909667.

References

1. Ross R. Atherosclerosis--an inflammatory disease. New Engl J Med. 1999; 340:115–26. [PubMed: 9887164]
2. Stocker R, Keaney JF Jr. New insights on oxidative stress in the artery wall. J Thromb Haemost: JTH. 2005; 3:1825–34.
3. Dopheide JF, Doppler C, Scheer M, Obst V, Radmacher MC, Radsak MP, et al. Critical limb ischaemia is characterised by an increased production of whole blood reactive oxygen species and expression of TREM-1 on neutrophils. Atherosclerosis. 2013; 229:396–403. [PubMed: 23880194]

4. Pu HL, Chiang WL, Maiti B, Liao ZX, Ho YC, Shim MS, et al. Nanoparticles with dual responses to oxidative stress and reduced ph for drug release and anti-inflammatory applications. ACS Nano. 2014; 8:1213–21. [PubMed: 24386907]
5. Grisham MB, Granger DN, Lefer DJ. Modulation of leukocyte-endothelial interactions by reactive metabolites of oxygen and nitrogen: relevance to ischemic heart disease. Free Radical Bio Med. 1998; 25:404–33. [PubMed: 9741579]
6. Wang Q, Tang XN, Yenari MA. The inflammatory response in stroke. J Neuroimmunol. 2007; 184:53–68. [PubMed: 17188755]
7. Hink U, Li H, Mollnau H, Oelze M, Matheis E, Hartmann M, et al. Mechanisms underlying endothelial dysfunction in diabetes mellitus. Circ Res. 2001; 88:E14–22. [PubMed: 11157681]
8. Brownlee M. Biochemistry and molecular cell biology of diabetic complications. Nature. 2001; 414:813–20. [PubMed: 11742414]
9. Giugliano D, Ceriello A, Paolisso G. Oxidative stress and diabetic vascular complications. Diabetes Care. 1996; 19:257–67. [PubMed: 8742574]
10. Kojda G, Harrison D. Interactions between NO and reactive oxygen species: pathophysiological importance in atherosclerosis, hypertension, diabetes and heart failure. Cardiovasc Res. 1999; 43:562–71. [PubMed: 10690328]
11. Petznick AM, Shubrook JH. Treatment of specific macrovascular beds in patients with diabetes mellitus. Osteopath Med Prim Care. 2010; 4:5. [PubMed: 20701768]
12. Steffen LM, Duprez DA, Boucher JL, Ershow AG, Hirsch AT. Management of Peripheral Arterial Disease. Diabetes Spectr. 2008; 21:171–7.
13. Peripheral arterial disease in people with diabetes. Diabetes Care. 2003; 26:3333–41. [PubMed: 14633825]
14. Jude EB, Oyibo SO, Chalmers N, Boulton AJ. Peripheral arterial disease in diabetic and nondiabetic patients: a comparison of severity and outcome. Diabetes Care. 2001; 24:1433–7. [PubMed: 11473082]
15. Ebrahimian TG, Heymes C, You D, Blanc-Brude O, Mees B, Waeckel L, et al. NADPH oxidase-derived overproduction of reactive oxygen species impairs postischemic neovascularization in mice with type 1 diabetes. Am J Pathol. 2006; 169:719–28. [PubMed: 16877369]
16. Ceradini DJ, Yao D, Grogan RH, Callaghan MJ, Edelstein D, Brownlee M, et al. Decreasing intracellular superoxide corrects defective ischemia-induced new vessel formation in diabetic mice. J Biol Chem. 2008; 283:10930–8. [PubMed: 18227068]
17. Rivard A, Silver M, Chen D, Kearney M, Magner M, Annex B, et al. Rescue of diabetes-related impairment of angiogenesis by intramuscular gene therapy with adeno-VEGF. Am J Pathol. 1999; 154:355–63. [PubMed: 10027394]
18. Joe B, Vijaykumar M, Lokesh BR. Biological properties of curcumin-cellular and molecular mechanisms of action. Crc Cr Rev Food Sci. 2004; 44:97–111.
19. Singh S, Aggarwal BB. Activation of transcription factor NF-kappa B is suppressed by curcumin (diferuloylmethane) [corrected]. J Biol Chem. 1995; 270:24995–5000. [PubMed: 7559628]
20. Barzegar A, Moosavi-Movahedi AA. Intracellular ROS protection efficiency and free radical-scavenging activity of curcumin. PLOS One. 2011; 6:e26012. [PubMed: 22016801]
21. Avci G, Kadioglu H, Sehirli AO, Bozkurt S, Guclu O, Arslan E, et al. Curcumin protects against ischemia/reperfusion injury in rat skeletal muscle. J Surg Res. 2012; 172:e39–46. [PubMed: 22079841]
22. Rogers NM, Stephenson MD, Kitching AR, Horowitz JD, Coates PT. Amelioration of renal ischaemia-reperfusion injury by liposomal delivery of curcumin to renal tubular epithelial and antigen-presenting cells. Brit J Pharmacol. 2012; 166:194–209. [PubMed: 21745189]
23. Anand P, Kunnumakkara AB, Newman RA, Aggarwal BB. Bioavailability of curcumin: problems and promises. Mol Pharm. 2007; 4:807–18. [PubMed: 17999464]
24. Altunbas A, Lee SJ, Rajasekaran SA, Schneider JP, Pochan DJ. Encapsulation of curcumin in self-assembling peptide hydrogels as injectable drug delivery vehicles. Biomaterials. 2011; 32:5906–14. [PubMed: 21601921]

25. Sun D, Zhuang X, Xiang X, Liu Y, Zhang S, Liu C, et al. A novel nanoparticle drug delivery system: the anti-inflammatory activity of curcumin is enhanced when encapsulated in exosomes. Mol Ther. 2010; 18:1606–14. [PubMed: 20571541]
26. Shahani K, Swaminathan SK, Freeman D, Blum A, Ma L, Panyam J. Injectable sustained release microparticles of curcumin: a new concept for cancer chemoprevention. Cancer Res. 2010; 70:4443–52. [PubMed: 20460537]
27. Zhu G, Mallery SR, Schwendeman SP. Stabilization of proteins encapsulated in injectable poly (lactide- co-glycolide). Nat Biotechnol. 2000; 18:52–7. [PubMed: 10625391]
28. Vert M, Li S, Garreau H. More About the Degradation of La/Ga-Derived Matrices in Aqueous-Media. J Control Release. 1991; 16:15–26.
29. Jeffery H, Davis SS, Ohagan DT. The Preparation and Characterization of Poly(Lactide-Co-Glycolide) Microparticles .1. Oil-in-Water Emulsion Solvent Evaporation. Int J Pharm. 1991; 77:169–75.
30. Napoli A, Valentini M, Tirelli N, Muller M, Hubbell JA. Oxidation-responsive polymeric vesicles. Nat Mater. 2004; 3:183–9. [PubMed: 14991021]
31. Reddy ST, Rehor A, Schmoekel HG, Hubbell JA, Swartz MA. In vivo targeting of dendritic cells in lymph nodes with poly(propylene sulfide) nanoparticles. J Control Release. 2006; 112:26–34. [PubMed: 16529839]
32. Hu P, Tirelli N. Scavenging ROS: superoxide dismutase/catalase mimetics by the use of an oxidation-sensitive nanocarrier/enzyme conjugate. Bioconjugate Chem. 2012; 23:438–49.
33. Velluto D, Demurtas D, Hubbell JA. PEG-b-PPS diblock copolymer aggregates for hydrophobic drug solubilization and release: cyclosporin A as an example. Mol Pharm. 2008; 5:632–42. [PubMed: 18547055]
34. Gupta MK, Meyer TA, Nelson CE, Duvall CL. Poly(PS-b-DMA) micelles for reactive oxygen species triggered drug release. J Control Release. 2012; 162:591–8. [PubMed: 22889714]
35. Gupta MK, Martin JR, Werfel TA, Shen T, Page JM, Duvall CL. Cell Protective, ABC triblock polymer-based thermoresponsive hydrogels with ROS-triggered degradation and drug release. J Am Chem Soc. 2014; 136:14896–902. [PubMed: 25254509]
36. Purcell BP, Lobb D, Charati MB, Dorsey SM, Wade RJ, Zellars KN, et al. Injectable and bioresponsive hydrogels for on-demand matrix metalloproteinase inhibition. Nat Mater. 2014; 13:653–61. [PubMed: 24681647]
37. Wilson DS, Dalmasso G, Wang L, Sitaraman SV, Merlin D, Murthy N. Orally delivered thioketal nanoparticles loaded with TNF-alpha-siRNA target inflammation and inhibit gene expression in the intestines. Nat Mater. 2010; 9:923–8. [PubMed: 20935658]
38. Lee D, Bae S, Hong D, Lim H, Yoon JH, Hwang O, et al. H2O2-responsive molecularly engineered polymer nanoparticles as ischemia/reperfusion-targeted nanotherapeutic agents. Sci Rep. 2013; 3:2233. [PubMed: 23868607]
39. Poole KM, Tucker-Schwartz JM, Sit WW, Walsh AJ, Duvall CL, Skala MC. Quantitative optical imaging of vascular response in vivo in a model of peripheral arterial disease. Am J Physiol-Heart C. 2013; 305:H1168–80.
40. Convertine AJ, Benoit DS, Duvall CL, Hoffman AS, Stayton PS. Development of a novel endosomolytic diblock copolymer for siRNA delivery. J Control Release. 2009; 133:221–9. [PubMed: 18973780]
41. Nagai A, Koike N, Kudo H, Nishikubo T. Controlled Thioacyl Group Transfer (TAGT) Polymerization of Cyclic Sulfide:3 Novel Approach to AB Diblock Copolymers by the Combination of RAFT and TAGT Polymerizations. Macromolecules. 2007; 40:8129–31.
42. Fundueanu G, Constantin M, Stanciu C, Theodoridis G, Ascenzi P. pH- and temperature-sensitive polymeric microspheres for drug delivery: the dissolution of copolymers modulates drug release. J Mater Sci-Mater M. 2009; 20:2465–75. [PubMed: 19562468]
43. Hogg N, Darley-Usmar VM, Wilson MT, Moncada S. Production of hydroxyl radicals from the simultaneous generation of superoxide and nitric oxide. Biochem J. 1992; 281 (Pt 2):419–24. [PubMed: 1310595]

44. Kuzkaya N, Weissmann N, Harrison DG, Dikalov S. Interactions of peroxynitrite, tetrahydrobiopterin, ascorbic acid, and thiols: implications for uncoupling endothelial nitric-oxide synthase. J Biol Chem. 2003; 278:22546–54. [PubMed: 12692136]
45. Joshi RV, Nelson CE, Poole KM, Skala MC, Duvall CL. Dual pH- and temperature-responsive microparticles for protein delivery to ischemic tissues. Acta Biomater. 2013; 9:6526–34. [PubMed: 23402764]
46. Lorsbach RB, Murphy WJ, Lowenstein CJ, Snyder SH, Russell SW. Expression of the Nitric-Oxide Synthase Gene in Mouse Macrophages Activated for Tumor-Cell Killing - Molecular-Basis for the Synergy between Interferon-Gamma and Lipopolysaccharide. J Biol Chem. 1993; 268:1908–13. [PubMed: 7678412]
47. Mosser DM, Edwards JP. Exploring the full spectrum of macrophage activation. Nat Rev Immunol. 2008; 8:958–69. [PubMed: 19029990]
48. Like AA, Rossini AA. Streptozotocin-induced pancreatic insulitis: new model of diabetes mellitus. Science. 1976; 193:415–7. [PubMed: 180605]
49. Couffinhal T, Silver M, Zheng LP, Kearney M, Witzenbichler B, Isner JM. Mouse model of angiogenesis. Am J Pathol. 1998; 152:1667–79. [PubMed: 9626071]
50. Poole, KM.; Patil, CA.; Nelson, CE.; McCormack, DR.; Madonna, MC.; Duvall, CL., et al. SPIE Photonics West. San Francisco, CA: SPIE; 2014. Longitudinal study of arteriogenesis with swept source optical coherence tomography and hyperspectral imaging; p. 89341Z-Z-7
51. Kundu K, Knight SF, Willett N, Lee S, Taylor WR, Murthy N. Hydrocyanines: a class of fluorescent sensors that can image reactive oxygen species in cell culture, tissue, and in vivo. Angew Chem Int Edit. 2009; 48:299–303.
52. Palmer GM, Fontanella AN, Shan S, Hanna G, Zhang G, Fraser CL, et al. In vivo optical molecular imaging and analysis in mice using dorsal window chamber models applied to hypoxia, vasculature and fluorescent reporters. Nat Protoc. 2011; 6:1355–66. [PubMed: 21886101]
53. Shonat RD, Wachman ES, Niu W, Koretsky AP, Farkas DL. Near-simultaneous hemoglobin saturation and oxygen tension maps in mouse brain using an AOTF microscope. Biophys J. 1997; 73:1223–31. [PubMed: 9284290]
54. Sorg BS, Moeller BJ, Donovan O, Cao Y, Dewhirst MW. Hyperspectral imaging of hemoglobin saturation in tumor microvasculature and tumor hypoxia development. J Biomed Opt. 2005; 10:44004. [PubMed: 16178638]
55. Poole KM, McCormack DR, Patil CA, Duvall CL, Skala MC. Quantifying the vascular response to ischemia with speckle variance optical coherence tomography. Biomed Opt Express. 2014 Accepted.
56. Mariampillai A, Standish BA, Moriyama EH, Khurana M, Munce NR, Leung MK, et al. Speckle variance detection of microvasculature using swept-source optical coherence tomography. Opt Lett. 2008; 33:1530–2. [PubMed: 18594688]
57. Yousefi S, Qin J, Zhi Z, Wang RK. Label-free optical lymphangiography: development of an automatic segmentation method applied to optical coherence tomography to visualize lymphatic vessels using Hessian filters. J Biomed Opt. 2013; 18:86004. [PubMed: 23922124]
58. Rosenkranz B, Winkelmann BR, Parnham MJ. Clinical pharmacokinetics of molsidomine. Clin Pharmacokinet. 1996; 30:372–84. [PubMed: 8743336]
59. Zhang YM, Wang H, Li JR, Jimenez DA, Levitan ES, Aizenman E, et al. Peroxynitrite-induced neuronal apoptosis is mediated by intracellular zinc release and 12-lipoxygenase activation. J Neurosci. 2004; 24:10616–27. [PubMed: 15564577]
60. Amoli MM, Mousavizadeh R, Sorouri R, Rahmani M, Larijani B. Curcumin inhibits in vitro MCP-1 release from mouse pancreatic islets. Transplant P. 2006; 38:3035–8.
61. Wang Y, Rangan GK, Goodwin B, Tay YC, Harris DC. Lipopolysaccharide-induced MCP-1 gene expression in rat tubular epithelial cells is nuclear factor-kappaB dependent. Kidney Int. 2000; 57:2011–22. [PubMed: 10792620]
62. Tojo T, Ushio-Fukai M, Yamaoka-Tojo M, Ikeda S, Patrushev N, Alexander RW. Role of gp91(phox) (Nox2)-containing NAD(P)H oxidase in angiogenesis in response to hindlimb ischemia. Circulation. 2005; 111:2347–55. [PubMed: 15867174]

63. Wang YJ, Pan MH, Cheng AL, Lin LI, Ho YS, Hsieh CY, et al. Stability of curcumin in buffer solutions and characterization of its degradation products. J Pharmaceut Biomed. 1997; 15:1867–76.
64. O'Toole MG, Henderson RM, Soucy PA, Fasciotto BH, Hoblitzell PJ, Keynton RS, et al. Curcumin encapsulation in submicrometer spray-dried chitosan/Tween 20 particles. Biomacromolecules. 2012; 13:2309–14. [PubMed: 22738300]
65. Shahani K, Panyam J. Highly loaded, sustained-release microparticles of curcumin for chemoprevention. J Pharm Sci. 2011; 100:2599–609. [PubMed: 21547911]
66. May RC, Machesky LM. Phagocytosis and the actin cytoskeleton. J Cell Sci. 2001; 114:1061–77. [PubMed: 11228151]
67. Shive MS, Anderson JM. Biodegradation and biocompatibility of PLA and PLGA microspheres. Adv Drug Deliver Rev. 1997; 28:5–24.
68. Champion JA, Walker A, Mitragotri S. Role of particle size in phagocytosis of polymeric microspheres. Pharm Res. 2008; 25:1815–21. [PubMed: 18373181]
69. Hirosue S, Kourtis IC, van der Vlies AJ, Hubbell JA, Swartz MA. Antigen delivery to dendritic cells by poly(propylene sulfide) nanoparticles with disulfide conjugated peptides: Cross-presentation and T cell activation. Vaccine. 2010; 28:7897–906. [PubMed: 20934457]
70. Rhee SG. Cell signaling. H2O2, a necessary evil for cell signaling. Science. 2006; 312:1882–3. [PubMed: 16809515]
71. Hood ED, Chorny M, Greineder CF, ISA, Levy RJ, Muzykantov VR. Endothelial targeting of nanocarriers loaded with antioxidant enzymes for protection against vascular oxidative stress and inflammation. Biomaterials. 2014; 35:3708–15. [PubMed: 24480537]
72. Derochette S, Franck T, Mouithys-Mickalad A, Deby-Dupont G, Neven P, Serteyn D. Intra- and extracellular antioxidant capacities of the new water-soluble form of curcumin (NDS27) on stimulated neutrophils and HL-60 cells. Chem-Biol Interact. 2013; 201:49–57. [PubMed: 23291280]
73. Kim HW, Lin A, Guldberg RE, Ushio-Fukai M, Fukai T. Essential role of extracellular SOD in reparative neovascularization induced by hindlimb ischemia. Circ Res. 2007; 101:409–19. [PubMed: 17601801]
74. Urao N, Inomata H, Razvi M, Kim HW, Wary K, McKinney R, et al. Role of nox2-based NADPH oxidase in bone marrow and progenitor cell function involved in neovascularization induced by hindlimb ischemia. Circ Res. 2008; 103:212–20. [PubMed: 18583711]

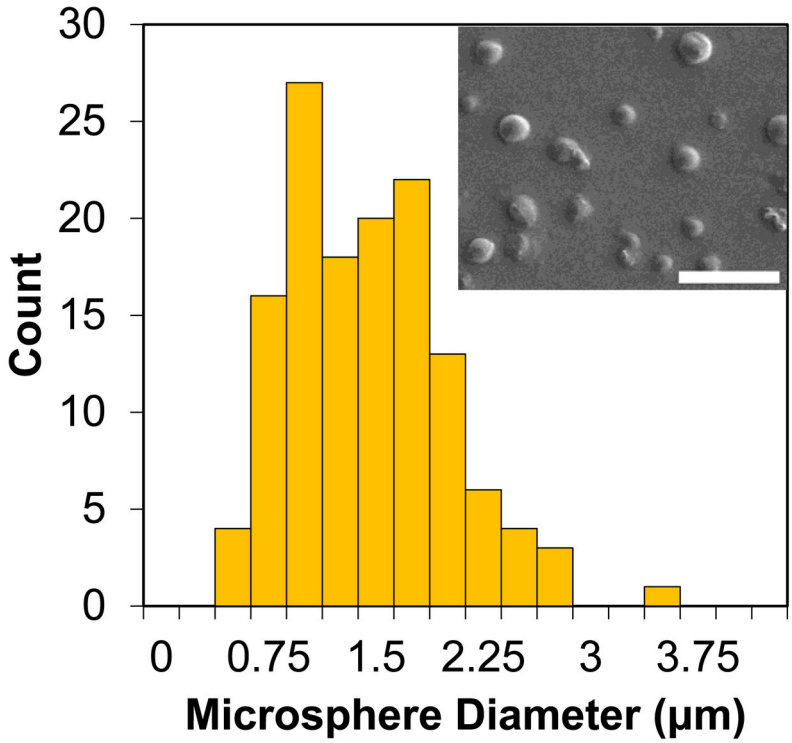

Fig. 1.

The size distribution of curcumin-PPS microspheres, as analyzed by SEM, indicated that average microparticle diameter was 1.33 μm with a standard deviation of 0.55 μm. Scale bar is 10 μm.

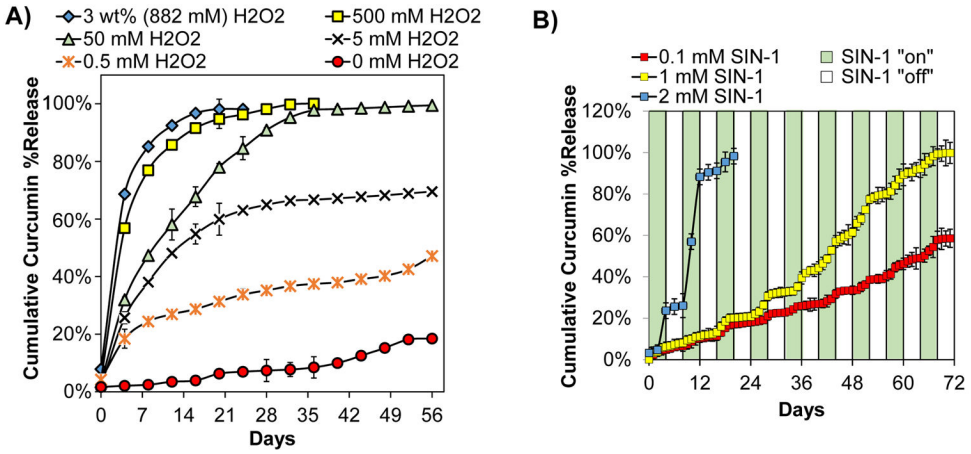

Fig. 2.

Curcumin release from PPS microparticles was ROS dose-dependent and on demand. A) *In vitro* release of curcumin from PPS microspheres exposed to temporally-constant H_2O_2 concentrations ranging from 0 mM to 3 wt% (882 mM) showed H_2O_2 dose-dependent release. B) *In vitro* release of curcumin from PPS microspheres with intermittent exposure to 0.1 mM, 1 mM, and 2 mM SIN-1 showed SIN-1 dose-dependent, on demand release during temporal phases when SIN-1 was present. n=3 for all samples.

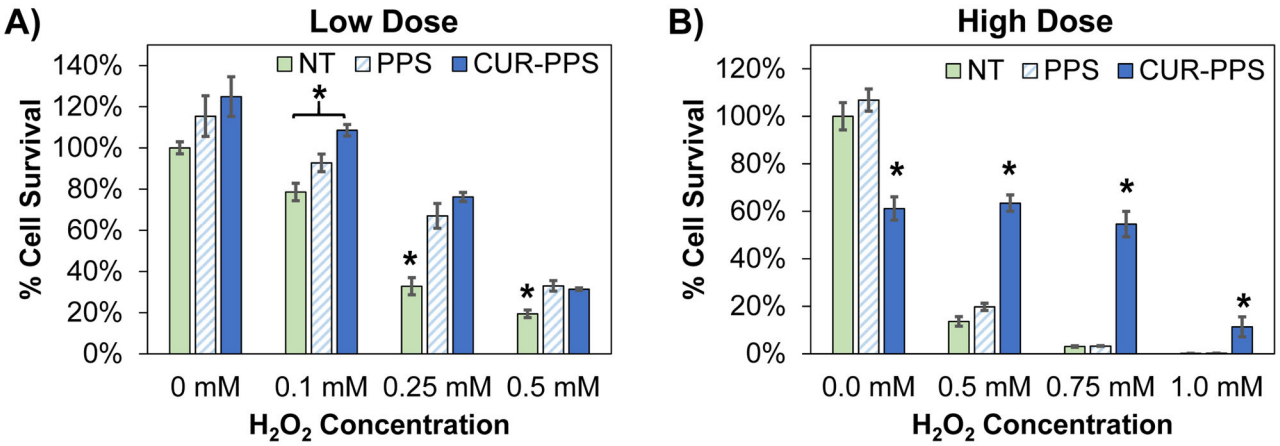

Fig. 3.

Curcumin loaded PPS microparticles reduce the cytotoxicity of H_2O_2. Cell survival was measured for luciferase-expressing 3T3 fibroblasts incubated for 24 hours with blank PPS microspheres, curcumin-PPS microspheres, or vehicle in media containing varied doses of H_2O_2. Curcumin dose is 3.4 μM in (A) and 27.1 μM in (B). Blank PPS microparticles represent the equivalent polymer dose (2.5 μg/mL PPS in (A) and 20.4 μg/mL PPS in (B)) used to deliver the corresponding curcumin dose. *$p<0.05$ relative to other treatment groups within each H_2O_2 dose. n=3 per group.

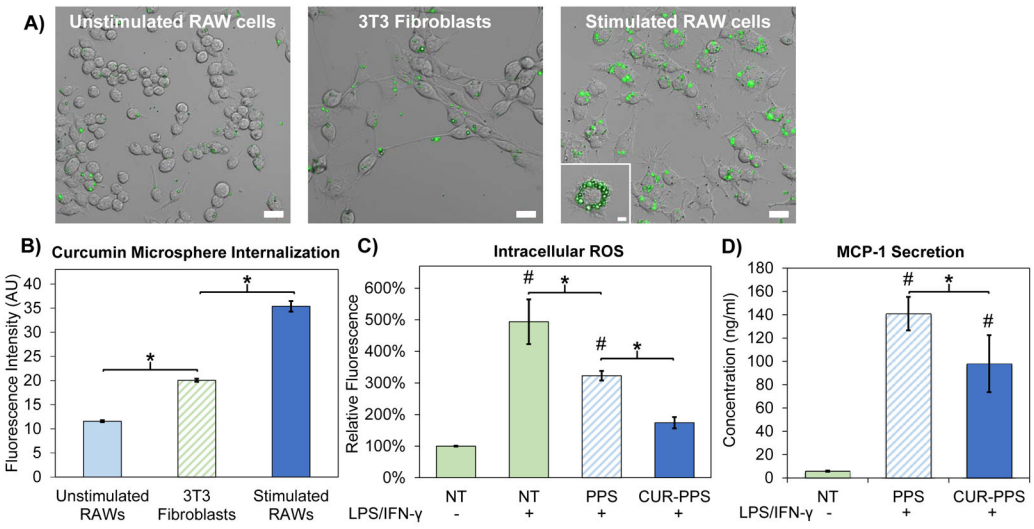

Fig. 4.

Curcumin-PPS microspheres are preferentially internalized by activated macrophages and exert functional effects on ROS generation and MCP-1 secretion. A) Confocal microscopy revealed that curcumin-PPS microspheres were internalized to a greater degree by LPS/IFN-γ stimulated RAW cells relative to non-activated macrophages and fibroblasts, suggesting size dependent targeting of the microparticles to pro-inflammatory macrophages. Scale bar is 20 μm. Inset in stimulated RAW macrophages is the center slice of a z-stack, confirming cell internalization of microspheres. Inset scale bar is 5 μm. B) Quantitative analysis of microsphere uptake was performed using flow cytometry to measure intracellular curcumin fluorescence, and significant differences were observed between all groups ($p<0.05$). C) Intracellular ROS levels are reduced in LPS/IFN-γ-stimulated RAW macrophages by treatment with PPS microspheres and Cur-PPS microspheres ($p<0.05$). Intracellular ROS levels in activated macrophages treated with CUR-PPS microspheres were statistically equivalent to the non-activated RAW cells. D) Secretion of MCP-1 is reduced in LPS/IFN-γ-stimulated RAW macrophages by treatment with Cur-PPS microspheres relative to blank PPS microspheres ($p<0.05$). Microsphere doses contain 3.4 μM curcumin or the equivalent polymer dose. *$p<0.05$ for differences between indicated groups. #$p<0.05$ relative to unstimulated macrophages (LPS/IFN-γ(−)/NT group).

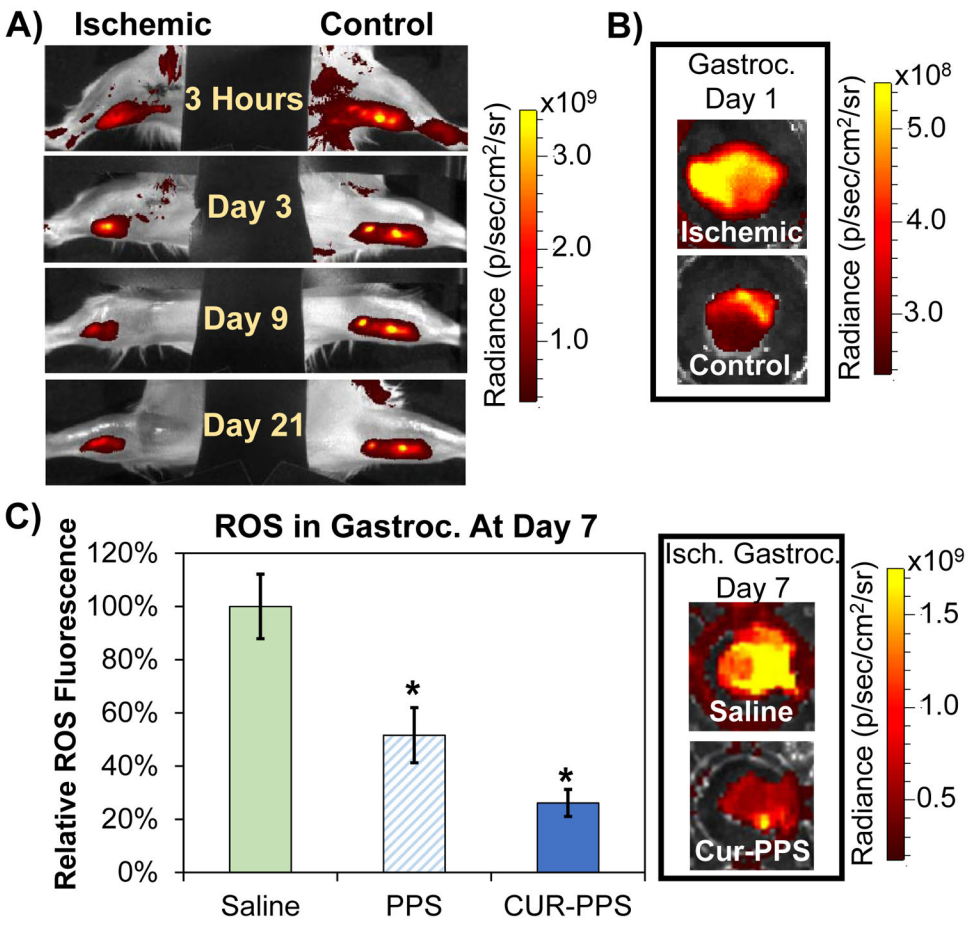

Fig. 5.

PPS microspheres provide sustained, on demand local curcumin release and reduce tissue ROS levels in the ischemic limb *in vivo.* A) Curcumin-PPS microspheres release curcumin more rapidly in the ischemic limb in comparison to the control limb. B) ROS levels in the gastrocnemius muscle are increased at day 1 post-surgery (level of ROS is 2.3-fold greater in ischemic versus control gastrocnemius). C) Blank PPS microspheres and curcumin-loaded PPS microspheres significantly reduce ROS in gastrocnemius muscles extracted from ischemic limbs. Data presented as mean ± SEM. Saline group n=8, blank PPS group n=11, curcumin-PPS group n=10. *$p<0.05$ relative to saline treatment.

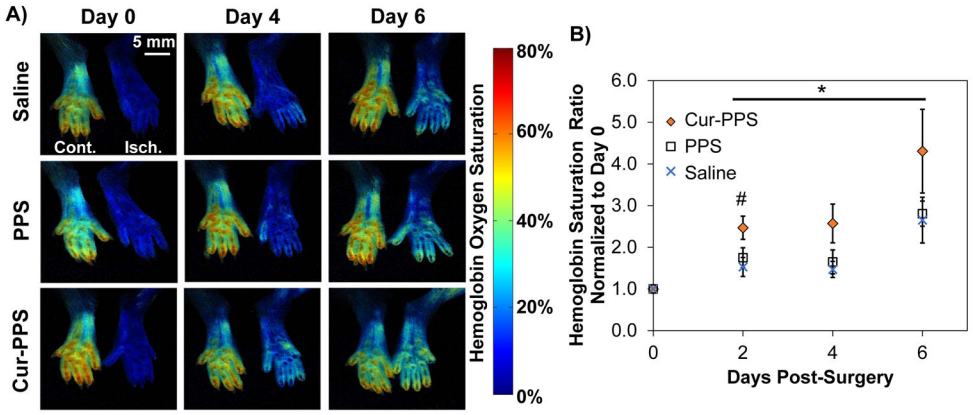

Fig. 6.

Curcumin-loaded PPS microspheres improved ischemic limb recovery in the setting of diabetes *in vivo*. A) Representative images from the time course of hemoglobin oxygen saturation recovery from each treatment group delivered to the ischemic limb of diabetic mice. B) Hemoglobin saturation is significantly increased in the curcumin-PPS treated group (n=10) relative to the blank PPS (n=11) and saline-treated (n=8) groups over the time course of ischemic recovery. At day 2, the curcumin PPS group has a significantly higher hemoglobin saturation ratio compared to the saline group. Data presented as mean ± SEM. *Cur-PPS group is significantly different from PPS and Saline groups over the time course from day 2 to 6 ($p<0.05$). PPS and Saline groups are not significantly different ($p>0.9$). #Cur-PPS and Saline differ significantly ($p<0.05$).

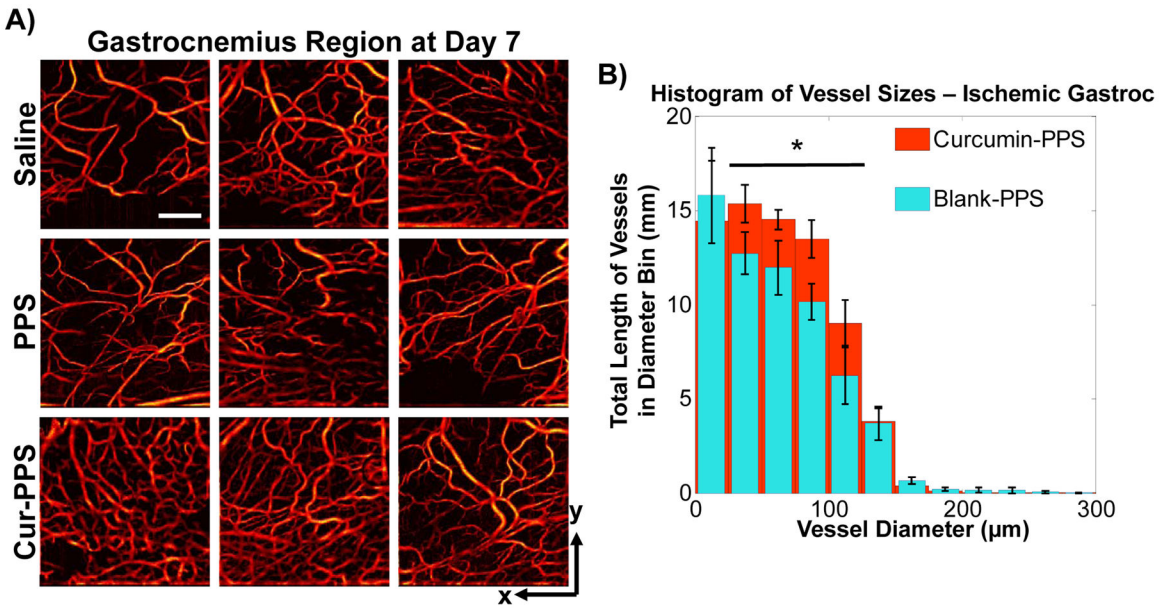

Fig. 7.

Vessel morphology was imaged non-invasively on day 7 with speckle variance OCT (n=4–5/group). A) Representative images of vessel morphology from each treatment group. Scale bar is 1 mm. B) Curcumin-PPS treated mice had a significant increase in length of vasculature with diameters between 25 μm and 125 μm relative to the blank PPS microsphere group ($p<0.05$).